Available online at www.sciencedirect.com
ScienceDirect
Trans. Nonferrous Met. Soc. China 33(2023) 3122−3131
Transactions of Nonferrous Metals Society of China
www.tnmsc.cn

Interaction and mechanism between arginine functionalized hydroxyapatite nanoparticles and human umbilical vein endothelial cells

Zi-chang LIN[1,2*], Bin-long CHEN[1,3*], Shi LIU[4*], Yan-yan HUANG[1], Yan-zhong ZHAO[1]

1. Health Management Center, The Third Xiangya Hospital, Central South University, Changsha 410013, China;
2. Department of Laboratory Medicine, The Third Xiangya Hospital, Central South University, Changsha 410013, China;
3. Department of Urology, The Third Xiangya Hospital, Central South University, Changsha 410013, China;
4. Clinical Class 6 of Grade 2019, Changsha Medical College, Changsha 410219, China

Received 4 November 2022; accepted 19 May 2023

Abstract: The interaction between terbium-doped arginine functionalized hydroxyapatite nanoparticles (Arg@HAP^{Tb} NPs) and cells, and the hindered endocytosis mechanisms of human umbilical vein endothelial cells (HUVECs) were studied by observing the cell uptake of Arg@HAP^{Tb} NPs with laser scanning confocal microscopy. Average fluorescence intensity of cells after uptaking different concentrations of NPs was determined by flow cytometer. The results indicate that internalized Arg@HAP^{Tb} NPs mainly exist in the cytoplasm of HUVECs, and most of them distribute around the cell nuclei. The entrapment of Arg@HAP^{Tb} NPs shows time-dependent and concentration-dependent manners with optimal time of 4 h and concentration of 50 mg/L. Arginine modification significantly improves the uptake efficiency of HAP^{Tb} NPs. The entry of Arg@HAP^{Tb} NPs into HUVECs is mainly through concave protein-mediated endocytosis, an energy-dependent active transport process.

Key words: hydroxyapatite nanoparticles; transmembrane transport; arginine modification; endocytosis

1 Introduction

Nanoparticles (NPs) have been widely used as delivery carriers due to their unique chemo-physical properties [1]. Many evidences have demonstrated the potential capacity of NPs to bind, concentrate and protect DNA [2]. Recently, hydroxyapatite (HAP) NPs have attracted considerable attention as new candidate of nonviral vectors for gene therapy due to their excellent properties [3]. However, how to improve transfection efficiency is the core issue of all non-viral vector research [4,5]. As intracellular endocytosis and transport process are the determining factors of gene transfection rate [6,7], exploring the interactive mechanism between arginine functionalized HAP NPs (Arg@HAP^{Tb} NPs) and cells is urgent for the rational design and construction of Arg@HAP^{Tb} NPs-based gene vectors [8]. At present, several possible pathways such as endocytosis, non-endocytosis and direct entry into cell membrane have been reported for explaining the mechanism of transmembrane transport of NPs. But most researchers prefer the dominant role of endocytosis [9]. Endocytosis is generally divided into phagocytosis and endocytosis according to the vesicles size formed by endocytosis substances or the components taken by cells [10]. Endocytosis in mammalian cells is mainly divided into clathrin-mediated endocytosis [11,12], small-concave protein-mediated endocytosis [13], and macropinocytosis [14]. In addition to the clathrin

* These authors contributed equally to this work
Corresponding author: Yan-zhong ZHAO, Tel: +86-731-88618138, E-mail: yanzhongzhao@163.com
DOI: 10.1016/S1003-6326(23)66322-8

and concave-mediated endocytosis, and macro-pinocytosis pathways, clathrin and concave independent endocytosis pathways have been found in cells under stimulation [15]. IRURZUN and CARRASCO [16] observed the entry of some viruses into cells in the form of unenveloped NPs (Sendai virus and influenza virus), but failed to draw a clear conclusion due to the lack of clear evidence such as molecular markers of this pathway. The cellular uptake and transport pathways of NPs are restricted by their physiochemical properties such as particle size, shape, surface charge, as well as cell types and other factors [17,18]. Especially, when NPs interacted with cells, endocytosis pathways of cellular entry and intracellular transport pathways need to be further studied. Considering the complex endocytosis mechanism and pathways to different NPs, it is very important to fully understand the interactive mechanism between NPs and cells and the entry pathways for the rational construction of Arg@HAP^{Tb} NPs-based gene vector.

In this study, human umbilical vein endothelial cells (HUVECs) were selected as the model cells. By combining with laser scanning confocal microscopy imaging and flow cytometry analysis, the interaction of terbium-doped Arg@HAP^{Tb} NPs with HUVECs was studied to explore and the endocytosis kinetics and mechanism of vascular HUVECs to Arg@HAP^{Tb} NPs. The aim of this study was to clarify the mechanism and further point out the direction for rational design and construction of Arg@HAP^{Tb} NPs based-gene vector.

2 Experimental

2.1 Materials

The experimental materials used in this experiment were as follows: HUVECs were taken from umbilical cords about 20 cm after cesarean section of healthy women in The Third Xiangya Hospital (Changsha, China) (informed consent of the women). Phosphate buffered saline (PBS), 4% paraformaldehyde (PFA) solution, inhibitors, 4′,6-diamidine-2-phenylindole (DAPI) storage solution were purchased from Sigma Company (USA). The confocal laser microscope (Carl Zeiss, Germany), and the flow cytometer (Beckman, USA) were applied in experiment.

2.2 Preparation of Arg@HAPTb NPs

Arg@HAP^{Tb} NPs were prepared according our previous work [3]. Briefly, a certain amount of Tb_2O_3 was weighed and completely dissolved in a certain amount of concentrated nitric acid, and then deionized water was added to prepare $Tb(NO_3)_3$ solution. A certain dose of $Ca(NO_3)_2{\cdot}4H_2O$ and $(NH_4)_2HPO_4$ was used for preparing solution, and then arginine (Arginine) was added to the phosphate solution. Next, $Tb(NO_3)_3$ solution was mixed with $Ca(NO_3)_2$ solution at 37 °C. Above mixed solution was added into $(NH_4)_2HPO_4$ solution at molar ratio (1:1.67) of $(Ca^{2+}+Tb^{3+})$/P under rapid stirring to pH 9.5. The above mixture was heated at 160 °C for 3 h. Finally, the emulsion was centrifuged and washed with double distilled water. The naturally dried precipitations were ground to obtain Arg@HAPTb NPs.

2.3 TEM observation

TECNAI G2−20ST transmission electron microscope (FEI Company, Netherland) was used to characterize the morphology and size of HAP and Arg@HAP^{Tb} NPs. The sample preparation process consisted of making powder solution and dropping it onto a special copper net covered with carbon film, drying it in the air and then putting it into transmission electron microscope (TEM) for observation. The basic morphology, particle size, distribution range and agglomeration of the prepared powder samples were observed under a certain magnification.

2.4 Preparation of HUVECs

Fresh umbilical cords were collected and HUVECs were obtained under sterile conditions in the ultra-clean workbench. The isolated cells were identified as HUVECs by immunofluorescence. HUVECs were suspended in the medium containing fetal bovine serum and inoculated into 25 cm^2 cell culture flask for 3−4 d. After digestion, the cells were centrifuged for 10 min at 1500 r/min at room temperature, then the supernatant was removed and dimethyl sulfoxide (DMSO) was added (5%−10%) into 1−2 mL tube for the cryopreservation. After being kept in 4 °C refrigerators for 2 h, and −75 °C overnight, the cells were stored in the liquid nitrogen. For cell recovery, cells were removed from liquid nitrogen and thawed in water bath at 37−41 °C. The cells were

sucked into 6 mL RPMI 1640 medium containing 15% calf serum. After centrifugation, supernatant was replaced by 6 mL RPMI 1640 medium. The cells were placed in 25 cm^2 culture flask for open culture at 37 °C. On the second day, the medium was replaced once according to the situation. After 1:9 passage, the cells grew into monolayers after 3−4 d. After another 1:3 passage, the cells grew into monolayers after 4 d.

2.5 Cell uptake kinetics for Arg@HAP^{Tb} NPs

HUVECs were cultured in RPMI 1640 medium containing 10% fetal bovine serum, 100 mg/L streptomycin and 100 U/mL penicillin at 37 °C in 5% CO_2 incubator. A glass substrate petri dish with 3 mL medium (dedicated for laser confocal microscopy) was placed in the incubator for 15 min. The medium was removed and HUVECs at logarithmic growth stage were inoculated in petri dishes at density of 2×10^4 cm^{-2}. The cells were placed in the incubator for 2 h to adhere to the wall. Then, 2−3 mL of cell-free RPMI 1640 medium was carefully added for continuous culture. After the cell fusion degree reached 80%, the cells were randomly divided into normal control group (without any treatment) and terbium-doped Arg@HAP^{Tb} NPs treatment group. The culture medium was discarded. 2 mL medium with serum containing Arg@HAP^{Tb} NPs suspension diluted at 50 mg/L was added into the culture dish of treatment group. After culturing at 37 °C for 4 h, culture medium was removed. Unbound Arg@HAP^{Tb} NPs were washed from the cell surface with cold PBS. 4% PFA was added to fix cells at room temperature for 30 min. The cells was washed with PBS 4 times, the cap was gently covered, and it was wrapped with tin foil. The glass plate was observed by confocal laser microscope. HUVECs were grown in a 12-well culture plate with a density of 1.0×10^5 per well. After adherence was complete, the medium was discarded and 1.5 mL of terbium-doped Arg@HAP^{Tb} NPs (50 mg/L) was added. After shaking the plate carefully, the medium was placed at 37 °C. The culture medium in the normal control group (without any treatment) and terbium-doped Arg@HAP^{Tb} NPs treated group (3 duplicate wells per group) were abandoned at 0.5, 1, 2, 4, and 6 h before washing with cold PBS for 3 times. Cells digested with 0.25% trypsin were used to measure the mean intracellular fluorescence intensity by flow cytometry, and the time dependence of uptake of Arg@HAP^{Tb} NPs by HUVECs endothelial cells was determined.

2.6 Intracellular distribution for Arg@HAP^{Tb} NPs and effects on cell proliferation

After cell fixation, plates were washed with PBS for 4 times, and 0.2 mL DAPI (100 ng/mL) was added to stain cell nuclei. After incubating at 37 °C for 15 min in 5% CO_2 incubator, the cells were washed with cold PBS for 4 times and wrapped in tin foil for inspection. The entry of terbium-doped Arg@HAP^{Tb} NPs into cells was observed under laser microscope. The distribution of Arg@HAP^{Tb} NPs into cells and their entry into the nuclei were investigated by means of the superposition of green fluorescence of terbium-doped Arg@HAP^{Tb} NPs and blue fluorescence of the nuclei. HUVECs were seeded into 96-well plates at a density of 3×10^4 per well and cultured for 24 h to enter into exponential growth period with 5 duplicate wells per group and a blank control group. 50 μL of HAP NPs and Arg@HAP^{Tb} NPs suspensions with different concentrations (0, 50, 100, and 200 mg/L) were added to the wells. After 4, 24, 48 and 72 h of culture, 20 μL of 5 mg/mL MTT preservation solution was added to each well, and the culture was continued for 4 h after shaking. The 100 μL mixture of ethanol and DMSO were added to each well and the shaking was performed at low speed for 8 min. Then, the optical density (OD) at 490 nm of each well was measured. The cell survival rate (R_s) was calculated by

$$R_s=\frac{OD_{Exp}-OD_B}{OD_C-OD_B}\times100\%$$

where OD_{Exp} is the OD value of experimental group, OD_B is the OD value of blank group, and OD_C is the OD value of control group. And the cytotoxicity of Arg@HAP^{Tb} NPs was evaluated based on the cell survival rate.

2.7 Effect of concentration and temperature on cellular uptake of Arg@HAP^{Tb} NPs

According to the method of cytodynamics experiment, the Arg@HAP^{Tb} NPs suspension with terbium doping at different concentrations (25, 50, 100, 150 mg/L) was added into the 12-well plates. Each well contained 1.5 mL HUVECs single cell

suspension. The cells were incubated at 37 °C for 4 h. The cells were digested by trypsin and the collected cells were subjected for average fluorescence intensity analysis using flow cytometry. Thus, the effect of Arg@HAP^{Tb} NPs concentration on the cell uptake was investigated using similar experimental method. The 50 mg/L terbium-doped Arg@HAP^{Tb} NPs suspension was added into the 12-well culture plates containing 1.5 mL HUVECs single cell suspension and incubated at 37 °C or 4 °C for 4 h, respectively. The average fluorescence intensity at two different temperatures was measured by flow cytometry.

2.8 Entry competition experiment of Arg@HAP^{Tb} NPs

HUVECs were incubated at 37 °C, 5% CO_2 for 1 h, and then were added with 50 mg/L Arg@HAP^{Tb} NPs suspension. Meanwhile, the same concentration of HAP^{Tb} NPs was used as the control group. Cells continued to be incubated in 5% CO_2 incubator for another 4 h. After the medium was removed, the cells were washed with cold PBS for 3 times. The cell entry of NPs in the two groups was observed with laser confocal microscopy, and the cell uptake efficiency was quantitatively analyzed by flow cytometry.

2.9 Transmembrane transport mechanism of Arg@HAP^{Tb} NPs

Based on the literature [19], biochemical inhibitors and the concentrations without toxic effect on HUVECs were selected. HUVECs were planted in 12-well plates with a density of 2.0×10^5 per well, and cultured at 37 °C and 5% CO_2. When the cell adhesion rate reached 80%, the medium was replaced by 100 mmol/L sodium azide (respiratory chain inhibitor), 10 mg/L chlorpromazine (clathrin-mediated endocytosis specific inhibitor), 1 mg/L philippine (caveolin-mediated endocytosis specific inhibitor), and 50 nmol/L wortmannin (macro-pinocytosis specific inhibitor). After incubation at 37 °C for 30 min, 50 mg/L terbium doped Arg@HAP^{Tb} NPs suspension was added, and the cells were incubated for another 4 h. The medium was removed and the cells were washed with cold PBS for 3 times. Cells in the control group were cultured for 4 h without any pretreatment but added with terbium-doped Arg@HAP NP suspension. The cell entry efficiency of Arg@HAP^{Tb} NPs was quantified by flow cytometry.

2.10 Statistical analysis

SPSS 10.0 statistical software was used for analysis. Each group was repeated for at least three times. The data were expressed as mean ± standard deviation ($X\pm S$). The results were analyzed by one-way ANOVA and LSD-t test. And $p<0.05$ was considered statistically significant.

3 Results and discussion

3.1 TEM observation of HAP NPs

The positive HAP powder in the acidic environment can bind negatively-charged DNA through electrostatic interaction. However, the low binding ability in neutral or weakly alkaline environment in vitro and in vivo makes it difficult to bind DNA. It has been found that of HAP powder with Zeta potential of (−12.5±6.5) mV was difficult to bind with negatively-charged DNA at pH 7.4. In this experiment, arginine is adopted to modify HAP NPs, because the hydrophilic arginine is a basic amino acid with guanidine-based group $—(CH_2)_3NHC(NH_2)^+$. The isoelectric point of 10.76 is higher than that of experimental condition. Thus, the NPs show positive charge in the whole reactive process. On the other hand, arginine containing the guanidine group can effectively penetrate the cell membrane [20], which is helpful for improving the efficiency of gene transfection.

TEM images show the short columnar and equiaxial HAP NPs synthesized by hydrothermal method. The length of the short rod-like NPs is 60−180 nm, the cross-sectional size of the same particle is 30−70 nm, and the aspect ratio of the short rod-like NPs is 2−4. The diameter of equiaxed NPs is about 30 nm. The hexagonal structure of HAP NPs also reflects the habit of HAP growing into rod and needle particles (Fig. 1(a)). In contrast, arginine modification significantly reduces the size of HAP NPs to 50−80 nm. Moreover, the size difference in each direction is small, and the shape of HAP NPs becomes irregular (Fig. 1(b)). These results demonstrate that arginine can inhibit the growth rate of HAP NPs to a certain extent.

3.2 Acquisition and identification of HUVECs

Vascular endothelial cells in the blood vessel

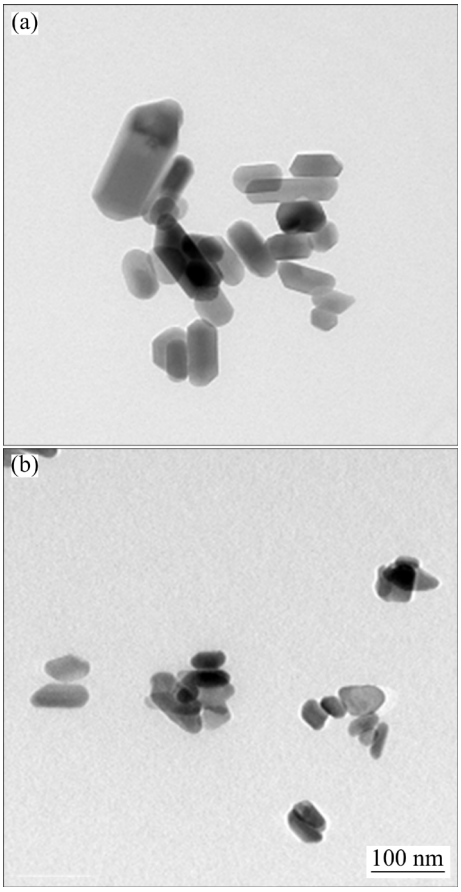

Fig. 1 TEM images of HAP^{Tb} NPs (a) and $Arg@HAP^{Tb}$ NPs (b)

lumen surface are the boundary between circulating blood and vessel wall barrier cells. As the main part of vessel wall, vascular architecture and physical condition of blood only contacted cells, it can absorb various biological macromolecules in the blood and transport nutrients to different parts, or translocate across the endothelium to the intima to meet their own or surrounding tissue nutritional needs. For $Arg@HAP^{Tb}$ NPs, vascular endothelial cells are the first barrier contacted by $Arg@HAP^{Tb}$ NPs when they were used as the gene transfection vector in vivo. Therefore, HUVECs are selected as the model cells to investigate the interaction between vascular and $Arg@HAP^{Tb}$ NPs. The morphology of HUVECs before and after passage is shown in Figs. 2(a, b), respectively. HUVECs are found to sparsely distribute in the plate before 48 h of passage. The cells with clear outline show the spindle shape. The increase of cell density slowly results in the polygonal formation with uniform morphology and single-layer growth (Fig. 2(b)). These results demonstrate that the monolayer adherent HUVECs are successfully obtained. Fluorescence imaging shows that strong green fluorescence is only observed in the cytoplasm of most cells treated with Arg@HAP NPs, but no cells with PBS treatment (Fig. 3).

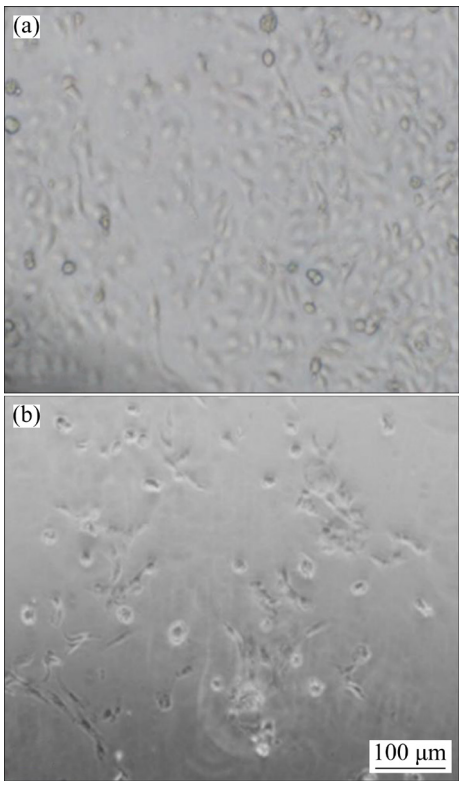

Fig. 2 Images of HUVECs before (a) and after (b) cell passage

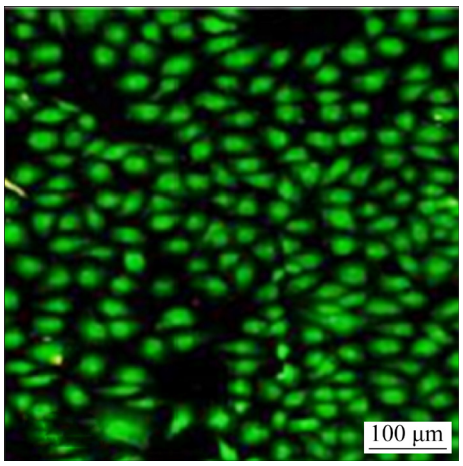

Fig. 3 HUVECs under fluorescence microscope

3.3 Cellular uptake distribution and kinetics of $Arg@HAP^{Tb}$ NPs

The laser confocal image of vascular endothelial cells incubated with $Arg@HAP^{Tb}$ NPs (50 mg/L) at 37 °C for 4 h is shown in Fig. 4. The localization and distribution of NPs in cells are

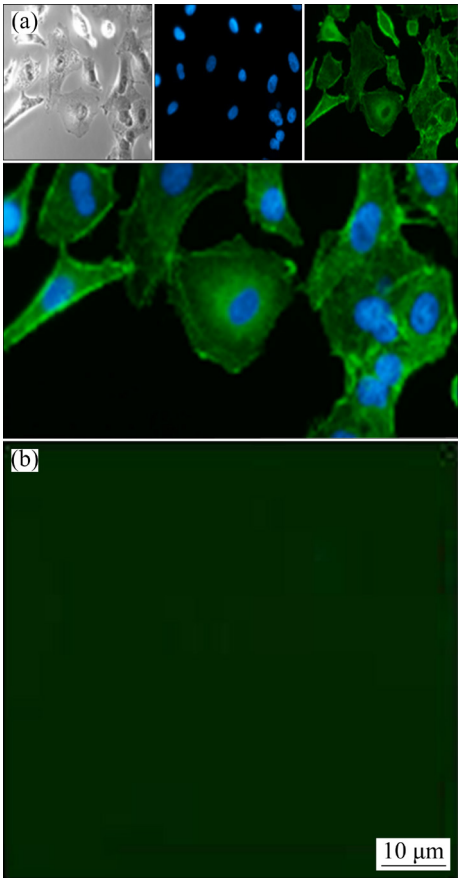

Fig. 4 Cell uptake images using confocal laser scanning microscopy: (a) Arg@HAP^{Tb} NPs (green) evident in cells stained with DAPI (blue); (b) Cells without Arg@HAP^{Tb} NPs incubation

clearly distinguished according to the green fluorescence emitted from terbium ion of Arg@HAP^{Tb} NPs. The cellular uptake and distribution of Arg@HAP^{Tb} NPs are quantitatively observed, suggesting that the Arg@HAP^{Tb} NPs doped with rare earth element terbium can distribute in the cytoplasm after efficiently entering into the cells. In addition, the green signal indicates that most of NPs accumulate around cell nuclei. Figure 4(a) shows the cell image under the bright field and the blue cell nuclei stained with DAPI under the laser confocal microscope. Besides, the green fluorescence in Fig. 4(a) illustrates the distribution of Arg@HAP^{Tb} NPs. Figure 4(b) shows the image of cell without Arg@HAP^{Tb} NPs incubation. As the laser confocal microscope can display a 3D-cross-sectional image of the cell to provide the information of NPs localization in the cell, it is adopted to observe whether terbium-doped Arg@HAP^{Tb} NPs are transported into the cell or only adsorbed on the cell surface. The fluorescence image indicates that Arg@HAP^{Tb} NPs doped with terbium enter into cell and distribute well in the cytoplasm. Most of the HAP/ARG NPs distribute around the nuclei.

As can be seen from Fig. 5, the uptake of Arg@HAP^{Tb} NPs by HUVECs shows a time-dependent manner. (33.02±6.14)% HUVECs emit green fluorescence after incubating with 50 mg/L Arg@HAP^{Tb} NPs for 4 h. The portion of HUVECs emitting green fluorescence reaches (85.25±3.15)% after 4 h of treatment and the proportion is merely increased by about 5% in the following 2 h, which may be due to the saturation of Arg@HAP^{Tb} NPs by cells. Therefore, 4−6 h is selected as the optimal time for the follow-up studies (Fig. 5).

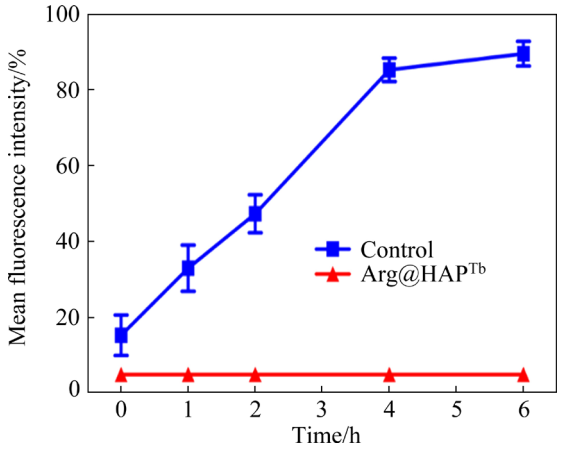

Fig. 5 Flow cytometry analysis of cell fluorescence intensity of cells with Arg@HAP^{Tb} NPs treatment

3.4 Effects of Arg@HAP^{Tb} NPs on cell proliferation

Next, the effect of HAP^{Tb} NPs and Arg@HAP^{Tb} NPs on the cell proliferation of HUVECs was investigated. The OD value of absorbance of HUVECs under different concentrations and time of Arg@HAP^{Tb} NPs was detected as the number of surviving cells was positively proportional to the absorbance value. MTT assay did not show statistical difference of viability for the cells with different treatment (p>0.05; Fig. 6). These results show the negligible low cytotoxicity effect of Arg@HAP^{Tb} NPs on the normal growth of HUVECs in vitro.

3.5 Effect of concentration and temperature on cellular uptake of Arg@HAP^{Tb} NPs

Next, the effect of Arg@HAP^{Tb} NPs concentration on the cell uptake was investigated.

FACS assay indicates that the fluorescence ratios of endothelial cells of Arg@HAP^{Tb} NPs are (33.42±5.61)%, (94.35±5.34)%, (92.47±4.73)% and (72.02±7.65)%, respectively. This result indicates that HUVECs can uptake Arg@HAP^{Tb} NPs in concentration-dependent manner in the range of 0−50 mg/L as the continuous increase of concentration does not affect cellular uptake (Fig. 7). Therefore, 50 mg/L is an appropriate concentration for cellular uptake of Arg@HAP^{Tb} NPs. In addition, it should be noted that although Arg@HAP^{Tb} NPs enter into HUVECs in time and concentration dependence manners, no significant difference is found for Arg@HAP^{Tb} NPs-contained cells when Arg@HAP^{Tb} NPs are incubated with cells for more than 4 h or with saturate concentration. This suggests that the optimal time and concentration should be considered for Arg@HAP^{Tb} NPs as a gene carrier in vivo.

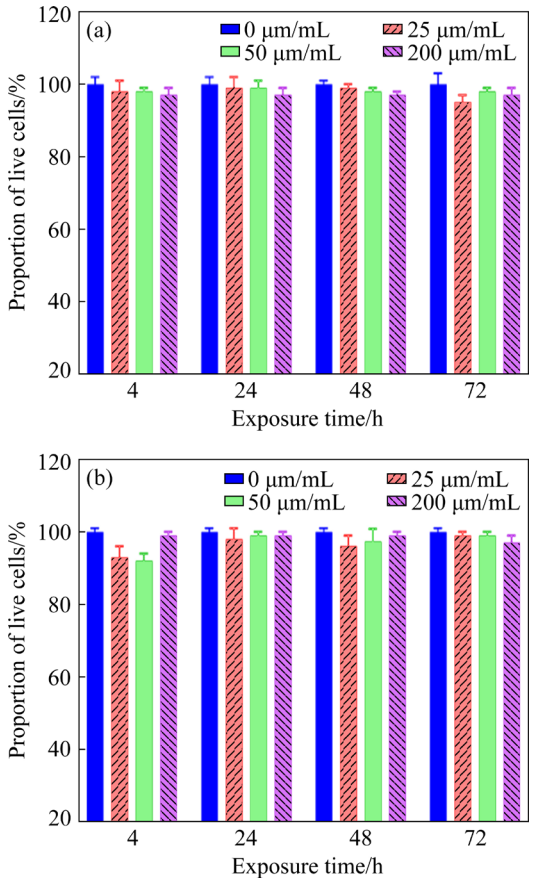

Fig. 6 Cell viability assay of HUVECs incubated with HAP^{Tb} NPs (a) and Arg@HAP^{Tb} NPs (b)

The cellular uptake of Arg@HAP^{Tb} NPs at 37 °C was 2-fold higher than that at 4 °C (Table 1). This indicates that Arg@HAP^{Tb} NPs mainly enter into cells via energy-dependent endocytosis [21], while part of NPs can be uptaken by physical adsorption or diffusion at 4 °C. In general, endocytosis is an energy-dependent process. Cells in a "dormant" state at low temperature can decrease endocytosis-mediated uptake process. Therefore, the cells cultured at 4 °C can reduce the binding effect of NPs with cell membrane, while the cells at 37 °C can result in the high cell uptake efficacy due to the normal metabolism and constant energy supply.

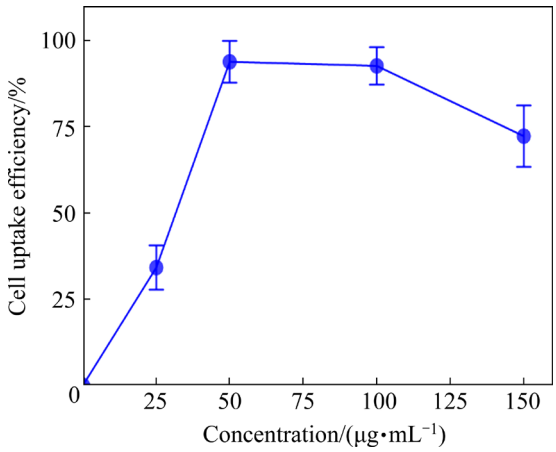

Fig. 7 Effect of concentration of Arg@HAP^{Tb} NPs on uptake by HUVECs

Table 1 Effect of incubation temperature on uptake of Arg@HAP^{Tb} NPs by HUVECs

Temperature/°C	Cell uptake of NPs/%
4	24.3±3.6
37	44.7±6.4

3.6 Entry competition and transmembrane transport mechanism of Arg@HAP^{Tb} NPs

By comparing the fluorescence intensity of HUVECs incubated with HAP^{Tb} NPs and Arg-modified HAP^{Tb} NPs, it is found that the signal in Arg@HAP^{Tb} NPs treated cells is much higher than that of HAP NPs treated cells (Fig. 8). This result clearly shows the improvement of arginine and its guanidine functional group on the cell uptake efficacy. In addition, compared with the normal control group, 10 mg/L chlorpromazine and 1 mg/L philippine reduce the cellular uptake of Arg@HAP^{Tb} NPs by 27.9% and 49.7%, respectively, while wortmannin at 50 nmol/L has no significant effect on this process, which suggests that both chlorpromazine and philippine can block the cellular uptake of Arg@HAP^{Tb} NPs [22]. Among

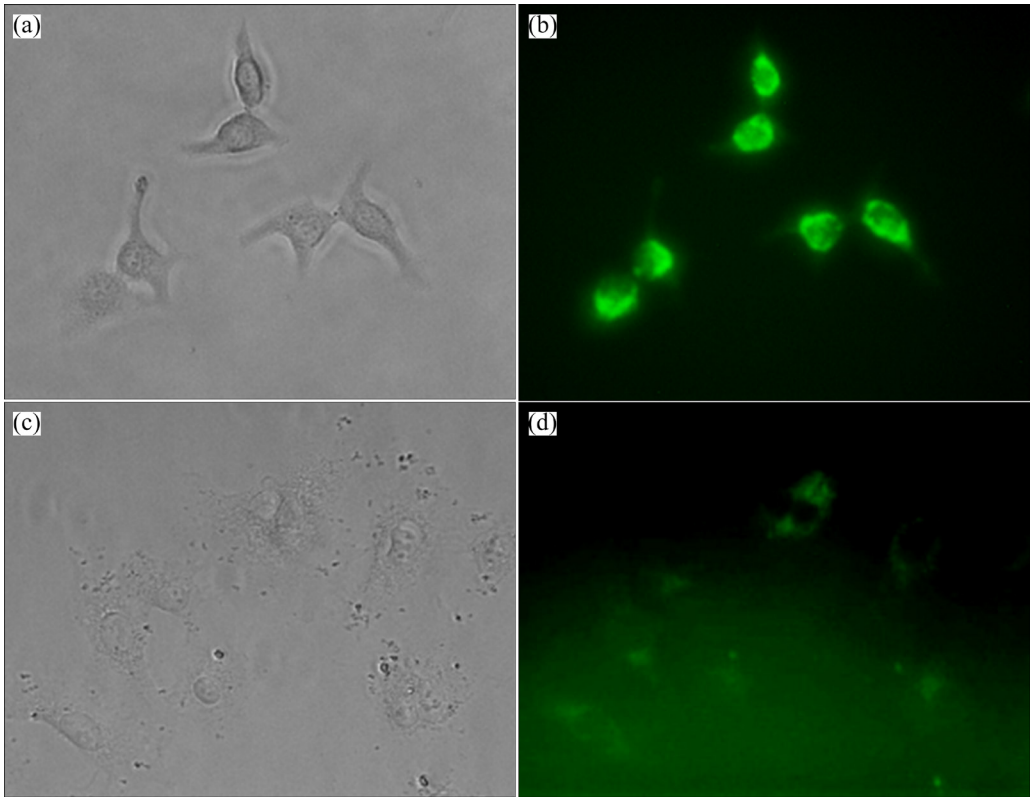

Fig. 8 Fluorescence images of cells incubated with arginine functionalized HAP^{Tb} NPs and arginine unfunctionalized HAP^{Tb} NPs: (a, b) $Arg@HAP^{Tb}$ NPs evident in HUVECs under fluorescence microscopy; (c, d) Unfunctionalized HAP^{Tb} NPs by arginine little evident in HUVECs

them, philippine inhibits the strongest effect on the cellular endocytosis. It was reported that the entry of exogenous virus into cells through caveolin-mediated endocytosis pathway could bypass the lysosome to avoid the degradation of substances [23]. Among them, guanidine functional group of arginine contained in the virus trans-membrane protein plays a key role in the caveolin-mediated endocytosis. Therefore, it is suspected that non-viral vector of HAP^{Tb} NPs modified with short arginine-rich peptides is more inclined to enter cells through the caveolin-dependent endocytosis pathway.

3.7 Transmembrane transport mechanism of $Arg@HAP^{Tb}$ NPs

Although the ability of $Arg@HAP^{Tb}$ NPs to enter into HUVECs has been demonstrated by cellular uptake experiments, the endocytic pathway that $Arg@HAP^{Tb}$ NPs are transported into HUVECs is not well understood. Here, a comprehensive study of the entry mechanism of $Arg@HAP^{Tb}$ NPs into HUVECs was performed by adopting different inhibitors of endocytosis. Inhibitor of sodium azide can reduce ATP production by inhibiting cytochrome oxidase in the mitochondrial electron transport chain, thereby causing cell energy shortage. Sodium azide pretreatment significantly decreases the uptake efficiency of HUVECs (Fig. 9), indicating energy-dependent uptake of $Arg@HAP^{Tb}$ NPs. Clathrin-mediated endocytosis is a classic endocytic pathway for animal cells to endocytosis exogenous substances. In this study, specific inhibitors of clathrin and caveolin mediated endocytosis pathway are used to further investigate their effect on the uptake of $Arg@HAP^{Tb}$ NPs. Figure 9 indicates that the cellular uptake efficiency of HUVECs to $Arg@HAP^{Tb}$ NPs is reduced by 27.9% and 49.7%, respectively, when the cells are pretreated by 10 mg/L chlorpromazine and 1 mg/L filipin group. However, no significant effect is found for the cells with 50 nmol/L Wortmannin pretreatment. This result shows that the energy-dependent entry of $Arg@HAP^{Tb}$ NPs into HUVECs occurs mainly through clathrin and caveolin mediated endocytosis.

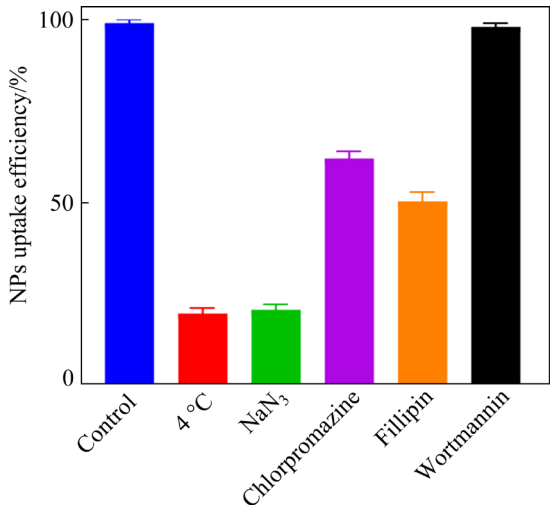

Fig. 9 Cellular uptake mechanism of Arg@HAP^{Tb} NPs

4 Conclusions

(1) The terbium-doped Arg@HAP^{Tb} NPs are found to mainly distribute in the cytoplasm of HUVECs, and most of them distribute around the cell nuclei after uptaking by HUVECs.

(2) The uptake process of Arg@HAP^{Tb} NPs is time-dependent and concentration-dependent with optimal time of 4 h and the optimal concentration of 50 mg/L. Meanwhile, arginine modification significantly increases the uptake efficiency of HAP^{Tb} NPs, which may be related to the effect of arginine and guanidine-based functional groups.

(3) Endocytosis inhibition assay shows that the entry of Arg@HAP^{Tb} NPs into HUVECs is an energy-dependent process, and the cell transmembrane transport mechanism is referred to clathrin and caveolin-mediated endocytosis, but caveolin-mediated endocytosis is the main pathway.

Acknowledgments

This work was supported by the Construction Program of Hunan Innovative Province (China)−High-tech Industry Science and Technology Innovation Leading Project (No. 2020SK2002), and Changsha Municipal Natural Science Foundation, China (No. kq2014265).

References

[1] WANG Xiao-huan, LI Long, SONG Fan. Interplay of nanoparticle properties during endocytosis [J]. Crystals, 2021, 11(7): 728−728.

[2] LIU Long-fei, ZHENG Meng-xi, LI Zhe, LI Qian, MAO Cheng-de. Patterning nanoparticles with DNA molds [J]. ACS Applied Materials and Interfaces, 2019, 11(15): 13853−13858.

[3] WANG Guo-hui, ZHAO Yan-zhong, TAN Juan, ZHU Shai-hong, ZHOU Ke-chao. Arginine functionalized hydroxyapatite nanoparticles and its bioactivity for gene delivery [J]. Transactions of Nonferrous Metals Society of China, 2015: 25(2): 490−496.

[4] STEINMAN N Y, CAMPOS L M, Feng Ya-kai, DOMB J A, HOSSEINKHANI H. Cyclopropenium nanoparticles and gene transfection in cells [J]. Pharmaceutics, 2020, 12(8): 768−768.

[5] ZHANG Yan, CHU Tian-jiao, SUN Le, CHEN Xiao-tong, ZHANG Wang-wang, ZHANG Hai-bin, HAN Bao-qin, CHANG Jing. Study on the transfection efficiency of chitosan-based gene vectors modified with poly-l-arginine peptides [J]. Journal of Biomedical Materials Research: Part A, 2020, 108(12): 2409−2420.

[6] FERIL L B. Ultrasound-mediated gene transfection [J]. Methods in Molecular Biology, 2009, 542: 179−94.

[7] LIU Cheng-jie, WU Wei, CHENG Yuan, YAO Wei, ZHEN Xu, JIANG Xi-qun. Transmembrane absorption and intracellular transport of macromolecules and nanoparticles [J]. Journal of Southeast University (Medical Science Edition), 2011, 30(1): 114−127. (in Chinese)

[8] MANZANARES D, CENA V. Endocytosis: The nanoparticle and submicron nano compounds gateway into the cell [J]. Pharmaceutics, 2020, 12(4): 371−371.

[9] SAHAY G, ALAKHOVA D Y, KABANOV A V. Endocytosis of nanomedicines [J]. Journal of Controlled Release, 2010, 145: 182−195.

[10] LIU Yong-kang, CHEN Guo-min. Transmembrane transport of macromolecules and granular materials by cell membrane [J]. Modern Medicine and Health, 2006, 22(5): 674−675. (in Chinese)

[11] KAKSONEN M, ROUX A. Mechanisms of clathrin-mediated endocytosis [J]. Nature Reviews: Molecular Cell Biology, 2018, 19(5): 313−326.

[12] PICCO A, KAKSONEN M. Quantitative imaging of clathrin-mediated endocytosis [J]. Current Opinion in Cell Biology, 2018, 53: 105−110.

[13] KOTOVA A, TIMONINA K, ZOIDL G R. Endocytosis of Connexin 36 is mediated by interaction with Caveolin-1[J]. International Journal of Molecular Sciences, 2020, 21(15): 5401−5401.

[14] COSTA VERDERA H, GITZ-FRANCOIS J J, SCHIFFELERS R M, VERDERA C H, GITZ-FRANCOIS J J, SCHIFFELERS R M, VADER P. Cellular uptake of extracellular vesicles is mediated by clathrin-independent endocytosis and macropinocytosis [J]. Journal of Controlled Release, 2017, 266: 100−108.

[15] RAHUL T, PRIYANKA J, SAKET A, HAIDER T, SONI V, PANDEY V. State-of-art based approaches for anticancer drug-targeting to nucleus [J]. Journal of Drug Delivery Science and Technology, 2018, 48: 383−392.

[16] IRURZUN A, CARRASCO L. Entry of poliovirus into cells is blocked by Valinomycin and Concanamycin A [J]. Biochemistry, 2001, 40(12): 3589−600.

[17] ZHU Mo-tao, NIE Guang-jun, MENG Huan, XIA-Tian, NEL

A, ZHAO Yu-liang. Physicochemical properties determine nanomaterial cellular uptake, transport, and fate [J]. Accounts of Chemical Research, 2013, 46(3): 622−631.
[18] GU Ning, LIN Xu-bo. Progress in simulation of the effect of medical nanoparticles on cell like membrane [J]. Advances in Biochemistry and Biological Physics, 2013, 40(10): 918−924. (in Chinese)
[19] TANG Hua-yuan, ZHANG Hong-Wu, YE Hong-fei, ZHENG Yong-gang. Receptor-mediated endocytosis of nanoparticles: Roles of shapes, orientations, and rotations of nanoparticles [J]. The Journal of Physical Chemistry B, 2018, 122: 171−180.
[20] TAKECHI H Y, SAITO H. Current understanding of physicochemical mechanisms for cell membrane penetration of arginine-rich cell penetrating peptides: Role of glycosaminoglycan interactions [J]. Current Protein and Peptide Science, 2018, 19(6): 623−630.
[21] ALLARD V E, HERVE-AUBERT K, KAAKI K, THIBAUT B, ANASTASIA S, KONSTANTIN V S, ANASTASIA A I, MARIE-LOUISE S, ALEXEY V F, IGOR C. Folic acid-capped pegylated magnetic nanoparticles enter cancer cells mostly via clathrin-dependent endocytosis [J]. Biochim Biophys Acta Gen Subj, 2017, 1861(6): 1578−1586.
[22] SCHNITZER J E, OH P, PINNEY E, ALLARD J. Filipin-sensitive caveolae mediated transport in endothelium: reduced transcytosis, scavenger endocytosis, and capillary permeability of select macromolecules [J]. Journal of Cell Biology, 1994, 127(5): 1217−1232.
[23] WANG L H, ROTHBERG K G, ANDERSON R G. Mis-assembly of clathrin lattices on endosomes reveals a regulatory switch for coated pit formation [J]. Journel of Cell Biology, 1993, 123(5): 123−1107.

精氨酸功能化羟基磷灰石纳米颗粒与人脐静脉内皮细胞的相互作用及机制

林子畅[1,2]，陈斌龙[1,3]，刘 石[4]，黄艳艳[1]，赵颜忠[1]

1. 中南大学 湘雅三医院 健康管理中心，长沙 410013；
2. 中南大学 湘雅三医院 检验科，长沙 410013；
3. 中南大学 湘雅三医院 泌尿外科，长沙 410013；
4. 长沙医学院 2019 级临床 6 班，长沙 410219

摘 要：选用铽掺杂的精氨酸修饰的羟基磷灰石纳米颗粒(Arg@HAP^{Tb} NPs)，探讨该纳米颗粒与细胞的相互作用以及 Arg@HAP^{Tb} NPs 在血管内皮细胞中的内吞机制。选取人脐静脉内皮细胞(HUVEC)作为研究的模型细胞，通过激光扫描共聚焦显微镜监测 Arg@HAP^{Tb} NPs 在细胞中的摄取情况，并通过细胞流速仪检测不同浓度下的细胞摄取后的平均荧光强度。结果表明，HUVEC 吸收 Arg@HAP^{Tb} NPs 后主要定位在细胞质中，并主要分布在细胞核周围。Arg@HAP^{Tb} NPs 的入胞过程具有时间和浓度依赖性，作用时间以 4 h 为宜，纳米颗粒的浓度以 50 mg/L 为最佳。Arg@HAP^{Tb} NPs 入胞量明显强于未经精氨酸修饰的 HAP^{Tb} NPs。Arg@HAP^{Tb} NPs 进入 HUVECs 是一个能量依赖的主动运输过程，通过小凹蛋白介导的内吞作用发生。

关键词：羟磷灰石纳米颗粒；跨膜转运；精氨酸修饰；内吞作用

(Edited by Bing YANG)